Journal of the Institute of Engineering
Volume 18, No. 1 Published: February 2025
ISSN: 1810-3383

Analysis of Rebar-Concrete Bond Strength Through Finite Element Modeling

Rajan Suwal [a], Sujan Chapagain [b]

[a] *Civil Engineering Department, Pulchowk Campus, Institute of Engineering, Tribhuvan University, Nepal*
[b] *Civil Engineering Department, Pulchowk Campus, Institute of Engineering, Tribhuvan University, Nepal*

Corresponding Author: [b] sujan978@gmail.com

Received: 2024-03-09 Revised: 2024-04-11 Accepted: 2024-06-13

Abstract:
A reinforced concrete section is comprised of enveloping concrete to which external load is applied and the reinforcing bars (rebars) which receive load from the concrete by bond mechanism. Finite Element Model (FEM) of reinforced concrete structures can produce realistic responses to simulate bond behavior. For computational speed and simulation efficiency, a simple but realistic bond-slip model is required. In this paper, a modified approach to Cohesive Zone Model (CZM) in ABAQUS is proposed with perfect bond between smooth rebar and concrete surfaces. This approach produced excellent results for six reference bond test specimens from two studies with short and long rebar bond lengths. The predicted load-displacement response from numerical simulation were very close to the experiment test results. The predicted bond strengths showed 98.6% and 95.9% match with test results for short and long bond lengths respectively.

Keywords: Bond strength, Concrete, Finite element modeling, Rebar-concrete bond

1. Introduction

Reinforced concrete structures are ubiquitous around the world due to the ease in construction practice to obtain desired forms and strengths of structures. Much of the strength of a concrete structures depends on the reinforcement bars (rebars) specifically placed to resist tensile or compressive or shear loads. Rebars ensure the necessary strength in reinforced concrete as a result of load transfer that occurs due to rebar-concrete bond mechanism. Bond mechanism is a widely studied topic in structural engineering with many approaches to approximate the mechanism by theoretical simplifications. However, the internal transfer of stress is difficult to quantify in physical experiments. This is primarily due to the limitations imposed by equipment/sensor able to measure the minute differences along the rebar geometry. Significant variations occur under rebar ribs along the length of just around 1 mm.

Researchers have tried to mitigate this limitation in experimental tests by instead opting for Finite Element Modeling (FEM) and Analysis (FEA) to simulate rebar-concrete bond [1, 2, 3, 4, 5, 6, 7]. The use of FEM software is preferred by researchers as it can avoid the hurdles of physical tests. A wide range of tests can be validated and calibrated numerically with output close to the physical test results. With advances in commercially available computational hardware and FEA software, complex material properties and physical phenomena can be modeled numerically with acceptable results. In this paper, the authors have used ABAQUS software to model bond phenomenon between ordinary reinforcement bars and concrete. For a good FEM of rebar-concrete bond behavior, reliable bond models are required to simulate the load transmission along the bond length. After calibration against a reference test, these FE models can be employed in a three-dimensional simulation. In this study, two reference studies from the literature have been taken to model for short bond length and long bond length. The results from FEA are compared to the results reported from the reference tests.

2. Literature Review

Bond-slip phenomenon in concrete is a complex mechanism which depends on many factors like concrete strength, rebar size, rebar strength, concrete cover to rebar, rebar rib geometry, bond length, confinement to rebar, etc. [8, 9, 10, 11] As a result of this bond mechanism, load transfer is possible between concrete material and the embedded rebar material. In a bonded rebar, this load transfer can be attributed to the bond mechanism taking place via three types of forces [10, 1] as shown in Figure 1:

- Chemical adhesion between the rebar steel body and surrounding concrete
- Friction acting along the embedded rebar surface and concrete surface
- Interlock/bearing of deformed rebars' projected ribs against concrete

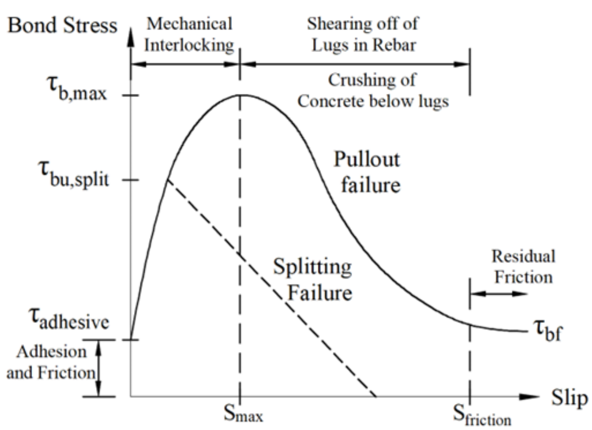

Figure 1: Bond-slip relationship in rebar bonded in concrete from Chapagain (2023)

When rebar is lightly loaded, slip (relative displacement) is resisted by the chemical force between rebar steel and concrete. Then a small slip occurs which is somewhat resisted by friction. But the majority of the deformed rebar's bond strength is a direct result of interlock/bearing of the ribs against concrete. With a further increase in tension load, slip increases and the rebar is stressed slowly until an ultimate bond stress is reached. After this, either concrete gets splitting cracks or the rebar gets pulled out. This overall action results in the bond mechanism. Many studies have been done to study the stress development near bonded rebars [9, 10, 1]. Figure 2 shows the stress concentration and crack development near a rebar due to various actions.

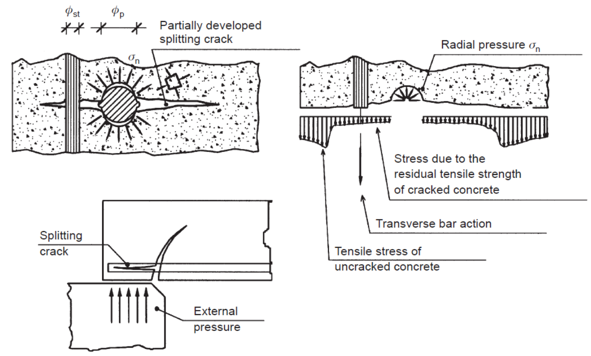

Figure 2: Splitting and confining actions around a deformed rebar from Plizzari et al (1998)

The overall bond mechanism of rebar embedded in concrete has been simulated using finite element software by many researchers with different approaches like traction-separation law for bond [1], 3D modeling of concrete and rebars including rib projections [12], spring connector elements for bond simulation [13], etc. This bond mechanism has been widely studied and many studies agree that the bond depends on several factors as listed earlier. But the studies differ on the assumed degree of dependence of the bond strength on those parameters [14].

3. Methodology

Researchers have used numerical analysis to simulate the complex bond mechanism in rebar and concrete materials via software like ANSYS [12, 15], ABAQUS [1, 6, 16, 5], etc. In this study, ABAQUS, a general-purpose finite element analysis suite, was used. In ABAQUS, material properties and geometry definitions have to be manually defined by the user [17].

3.1 Material property of concrete

CDP (Concrete Damaged Plasiticity) model feature in ABAQUS was used in this study to model non-linear behavior of concrete. In CDP model, user-defined stresses and inelastic strains are defined in the software to describe the non-linear property of concrete. CDP model is a smeared-crack continuous damage model in which concrete material may fail by crushing or cracking. In this study, the assumed CDPM values are 0.1 for flow potential eccentricity, a nominal value of 0.0001 for viscosity parameter, 30° for dilation angle ψ, 0.667 for K_c (shape factor for yield surface), and 1.16

for f_{b0}/f_{c0}. The CDP model does not support the concept of cracks developing at the material integration point. But ABAQUS can use the damage parameters to model concrete failure in tension as well as compression [17].

Input values for elasticity modulus, Poisson's ratio, stress values, cracking strain values, and the associated damage parameters at each cracking strain value are provided similar to the study done by Wahalathantri, Thambiratnam, Chan, and Fawzia (2011) [6]. The recommendations made in the paper are used in this study to define the stress-strain relationship in compression and tension. The response of concrete in uni-axial tension and uni-axial compression are characterized by CDP model are illustrated in Figure 3 [1]. Poisson's ratio was assumed as 0.2 [18]. Initially, it is assumed that concrete behaves linearly up to a stress at 50% of compressive strength σ_{cu} in the ascending branch. Then the stress value between the yield point at 0.5 σ_{cu} and 0.3 σ_{cu} in the descending branch of stress-strain curve is given as a function of strain by:

$$\sigma_c = \sigma_{cu} \frac{\beta\ (\varepsilon_c/\varepsilon_0)}{\beta - 1 + (\varepsilon_c/\varepsilon_0)^{\beta}}\ where,\ \beta = \left(1 - \frac{\sigma_{cu}}{\varepsilon_0\ E_0}\right)^{-1}$$

The parameter β depends on the shape of the stress-strain diagram with the strain at peak stress (ε_0) given by $\varepsilon_0 = 8.9 \times 10^{-5} \times \sigma_{cu} + 2.114 \times 10^{-3}$. The initial tangent modulus of elasticity is given by $E_0 = 124.31 \times \sigma_{cu} + 3283.12$, but in the above expressions, $\sigma_{cu}, \sigma_c, and E_0$ are in kip/in^2. Conversions to and from SI units are made for entry.

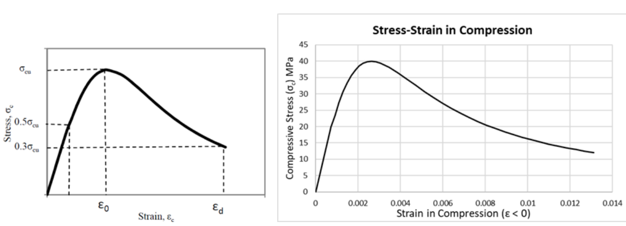

(a) Assumed stress-strain relation in compression and example

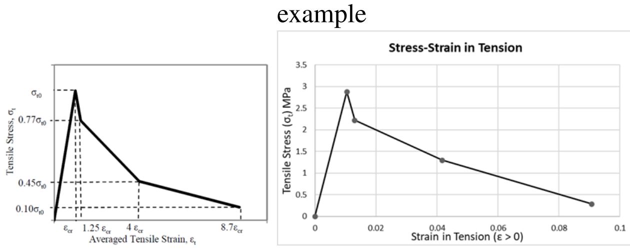

(b) Assumed stress-strain relation in tension and example

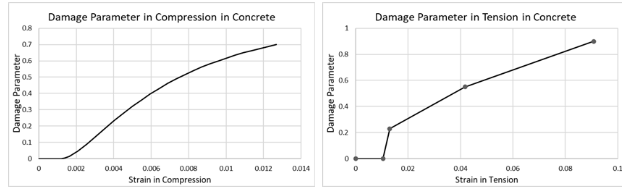

(c) Damage parameter progression in compression and tension

Figure 3: Stress-strain relationships and damage progression in FEM

Strain ε_d at 0.3 σ_{cu} in the descending portion is iteratively calculated using the non-linear stress-strain relationship. In this study, concrete in tension is assumed to behave elastically up to the failure stress σ_{t0} at strain ε_{cr} i.e., cracking in concrete at cracking stress and cracking strain. Then stress-strain curve drops to 0.77 σ_{t0} stress at strain 1.25 ε_{cr}. The stress is assumed to be 0.45 σ_{t0} at strain 4 ε_{cr} and 0.1 σ_{t0} stress at strain 8.7 ε_{cr} [6]. Figure 3 shows the stress-strain relationships and damage parameter progression in tension and compression. The damage parameter describes the degree of crushing and cracking in concrete. Its accuracy is checked by having the plastic strain as always positive and always increasing. In tension, for cracking strain ($\varepsilon_{cr} = \sigma_t/E_0$), the damage parameter is given by:

$$d_t = 0\ for\ \varepsilon_t < \varepsilon_{cr}\ and\ d_t = 1 - \frac{\sigma_t}{\sigma_{t0}}\ for\ \varepsilon_t \geq \varepsilon_{cr}$$

Similarly, in compression, the damage parameter is defined as:

$$d_c = 0\ for\ \varepsilon_c < \varepsilon_{c1}\ and\ d_c = 1 - \frac{\sigma_c}{\sigma_{cu}}\ for\ \varepsilon_c \geq \varepsilon_{c1}$$

3.2 Material property of rebars

To define the material property of steel rebars, expressions were taken from a previous study [1] which were in turn based on the expressions proposed by Yun and Gardner (2017) [19] for hot-rolled steel sections. But Chapagain (2023) showed that the proposed three-branch curve produce satisfactory results for steel rebars as well [1]. Based on the input of Young's modulus of elasticity (E), yielding stress (σ_y), and ultimate stress (σ_u), the engineering stress-strain curve may be obtained as:

- Linear Elastic ascending branch [19]

$$\sigma = E\varepsilon$$

- Strain-hardening flat branch [1]

$$\sigma = 1.01\sigma_y$$

- Non-linear ascending branch [19]

$$\sigma = \sigma_y + (\sigma_u - \sigma_y)\left[0.4\left(\frac{\varepsilon - \varepsilon_{sh}}{\varepsilon_u - \varepsilon_{sh}}\right) + 2\left(\frac{\varepsilon - \varepsilon_{sh}}{\varepsilon_u - \varepsilon_{sh}}\right)\left[1 + 400\left(\frac{\varepsilon - \varepsilon_{sh}}{\varepsilon_u - \varepsilon_{sh}}\right)^5\right]^{-\frac{1}{5}}\right]$$

- Post-failure descending branch [1] : After the ultimate stress failure, a drop is assumed to 0.1 σ_y at end strain = ultimate strain + 0.01.

Here, the ultimate strain is defined as:

$$\varepsilon = 0.6\left(1 - \frac{\sigma_y}{\sigma_u}\right) \textit{ but } \varepsilon_u \geq 0.06 \text{ for hot-rolled steels}$$

Similarly, the rebar strain corresponding to strain hardening branch is:

$$\varepsilon_{sh} = 0.1\left(\frac{\sigma_y}{\sigma_u}\right) - 0.0055 \text{ but } 0.015 \leq \varepsilon_{sh} \leq 0.03$$

Then an engineering stress-strain curve is obtained for any given rebar size using above expressions. The corresponding true stress-strain curve is subsequently obtained. A representative example of engineering stress-strain curve, true stress-strain curve, and plastic strain is shown in Figure 4 [1] for a #20 mm rebar.

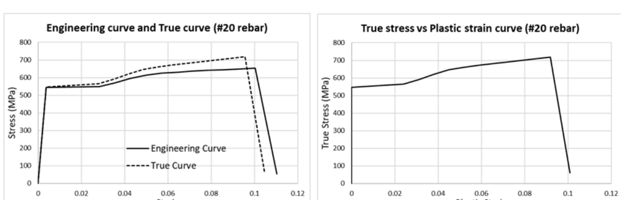

Figure 4: Engineering curve vs True curve; and True stress vs Plastic strain curve

3.3 Property of rebar-concrete bond

Different bond-slip laws have been proposed for various types of concrete and rebars [7, 10, 11, 18, 20]. In this study, Model Code 2010 was used to define the bond-slip relation for ABAQUS input. For deformed rebar, the bond stress (τ_b) between concrete and rebar for pull-out and splitting failure can be calculated in terms of the slip (s) according to fib Model Code 2010 (2013) [18] as shown in Table 1.

Table 1: (τ_b) vs (s) relation for deformed rebars (MC2010)

Part	Bond stress (τ_b) defined as	Range
I	$\tau_{b,max}(s/s_1)^{\alpha}$	$0 \leq s \leq s_1$
II	$\tau_{b,max}$	$s_1 \leq s \leq s_2$
III	$\tau_{b,max} - (\tau_{b,max} - \tau_{bf})\frac{s-s_2}{s_3-s_2}$	$s_2 \leq s \leq s_3$
IV	τ_{bf}	$s_3 < s$

The four parts of the bond-slip relation relate to the local crushing of concrete between rebar ribs, residual bond capacity as slip occurs, large relative displacement as concrete bond strength deteriorates, and residual bond strength due to confinement of the rebar respectively. α is recommended as 0.4 in the Model Code 2010 for unconfined concrete with good bond. Based on a previous study [1], the bond stress is assumed to drop to 0.99 τ_{bf} at s_2 relative displacement. This relation of bond stress and relative displacement defines the rebar-concrete relative moment and stress generation in the FEM as shown in an example of the defined bond-slip relation in Figure 5 [1].

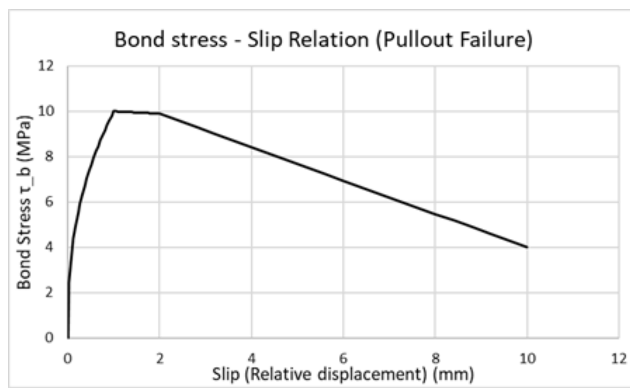

Figure 5: Bond-slip relation definition for ABAQUS

3.4 Parts and elements in FEM

Different element types are defined to model in the FEM. 2D wire truss elements are used to define embedded reinforcement bars (not considered in the reference studies for bond strength) in concrete mat/block. In 3D models for concrete as well as bonded reinforcement bars, C3D8R elements are used. These 3D solid elements are 8-noded brick elements with reduced integration. Several studies have shown the adequacy of C3D8R elements in ABAQUS for concrete modeling [2, 21, 22]. Then, material sections are assigned respective material properties. The parts are assembled to form a finite element model to simulate rebar bonded in concrete.

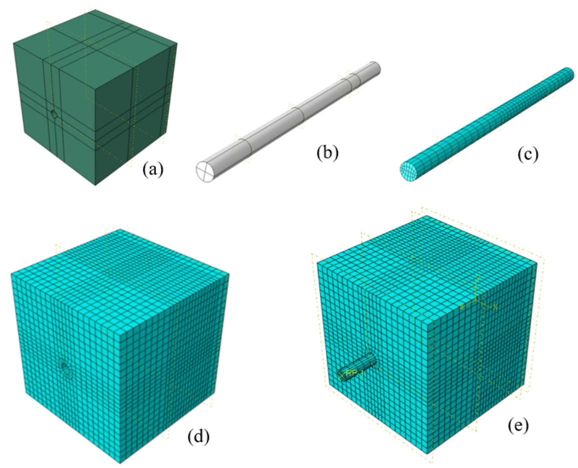

Figure 6: Example of parts definition in ABAQUS: (a) Concrete block part (b) Steel rebar part (c) Steel rebar mesh (d) Concrete block mesh (e) Meshed assembly of concrete block with bonded rebar

Figure 6 shows the representative example of C4-16-6d model from a reference test [23]. Mesh sizes are varied in this study depending on the expected stresses. Regions expected to be highly stressed are meshed finely, and regions far from expected high-stress regions are meshed coarsely. To obtain outputs, field output and history output requests are defined and set for specified units of time such that output requests produce approximately 12 results per mm displacement of rebar.

3.5 Parts interaction in FEM

Different types of contact between parts may be modeled in ABAQUS [17]. The node-to-surface type of contact is suitable for a surface in contact with a moving projectile-like body. The surface-to-surface type of contact is suitable for two body surfaces moving relative to each other but in contact with each other throughout. In this study, concrete material is assumed as a homogenous, isotropic material without any consideration of irregularities due to aggregates and cement paste matrix. Similarly, rebar's rib geometry is not considered.

For the assumed smooth rebar surface and surrounding uniform concrete body, the total bond mechanism is represented by the distribution of bond stress along the bond length alone. So, the surface-to-surface contact is used in this study. For contact between concrete and support, friction was considered and separation after contact was allowed. In ABAQUS, ”hard-contact” was assumed to generate infinite stiffness for overclosure at contact regions. Penetration of materials was also not allowed for all part interactions.

Along the rebar-concrete bond length, surface-based cohesive behavior was defined as a surface interaction property using Cohesive Zone Model (CZM) which utilizes traction-separation law [17]. After load application cohesion/bond failure along the rebar-concrete surface interface is defined by user-defined damage initiation of the cohesive stiffness. The CZM approach has been used by previous researchers with success [1, 2, 7]. This study adopts the approach proposed by Chapagain (2023) with an initial slip to $s_0 = 0.03$ mm occurring with a linear bond-slip relation instead of the curve defined as in Table 1 [1].

In ABAQUS, using the standard CZM approach, users cannot input a non-linear ascending branch of bond-slip relation. To get around this limitation, a linear ascending branch is defined until a very small slip of 0.03 mm occurs. After the initial linear branch, non-linear bond-slip curve data can be entered using the standard CZM approach. This modification in the data input allows a better representation of bond-slip relation without aditional computational power or programming difficulties. The results produced using this approach showed good results [1].

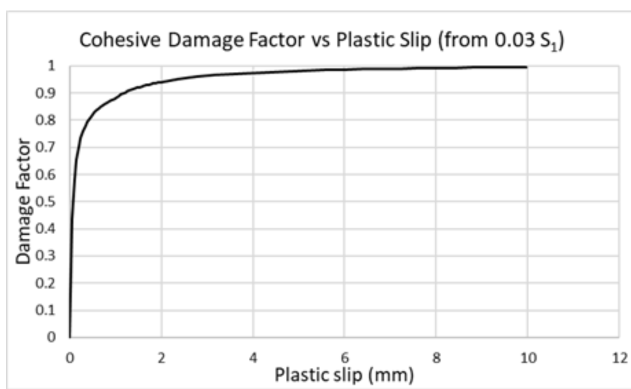

Figure 7: Example of the damage variable vs plastic slip plot in ABAQUS

For predicted stress $\overline{\sigma}$ with undamaged bond surface, the damage response at stress σ for any given rebar slip is characterized by damage variable (D). D = 0 for undamaged surface and D = 1 for fully damaged surface.

$$\sigma = (1-D)\overline{\sigma} \quad \text{i.e.,} \quad D = 1 - \frac{\sigma}{\overline{\sigma}}$$

An example for the damage evolution plotted against the plastic slip in bond surface is shown in Figure 7 [1]. Also, $\overline{\sigma} = K_{ss} \times$ Total slip, where $K_{ss} = K_{tt} = \tau_{max}/S_{max}$ is the stiffness coefficient of shear deformations. Stiffness coefficient of normal traction is taken as $K_{nn} = 100 \times K_{ss}$.

4. Results and Discussion

Two reference test studies were taken for FEA for short rebar bond length and long rebar bond length.

4.1 Reference test for short bond length

Khaksefidi, Ghalehnovi, and Brito (2021) conducted tests on 60 concrete blocks by having the bonded rebar in geometric center of the concrete block section [23]. The researchers tested for three different effective bond lengths ($2d_b$, $4d_b$, and $6d_b$). For rebar diameters of 12mm and 16mm, $200 \times 200 \times 200$ mm^3 concrete cubes had covers of 94mm and 92mm respectively. For 25 mm diameter rebars, $250 \times 250 \times 250$ mm^3 concrete cubes had 112.5 mm cover. The bond length was placed opposite from the loading end. In the tests, PVC pipes were used to prevent rebar bond with concrete except in the bond length. The mechanical properties of concrete and steel rebars reported in the study are shown in Table 2 and Table 3.

Table 2: Mean mechanical property of concrete in reference tests [23]

Concrete strength type	Compressive strength (MPa)	Split tensile strength (MPa)	Elasticity Modulus (GPa)
Normal	47.87	4.35	33.02

Table 3: Mean mechanical property of rebar in reference tests [23]

Rebar rib type designation	Yield stress (MPa)	Ultimate stress (MPa)	Elasticity Modulus (GPa)
AIV	600.3	743.3	243.51

A 3D analysis of four test specimens is carried out with the modified CZM approach. The peak bond strength was defined according to the reported test results [23]. S_3 value for bond-slip relation depends on the rebar geometry. In this study, S_3 was taken as 10mm for 16mm rebar and 15mm for 25mm rebar. Restrictive boundary condition was applied to the face near loading end, as shown in Figure 8 for C4-25-4d test specimen model and the test setup. The restraint offered by steel plate holding the concrete block in place was assumed to restrict in translation but not in rotation on the loading end face.

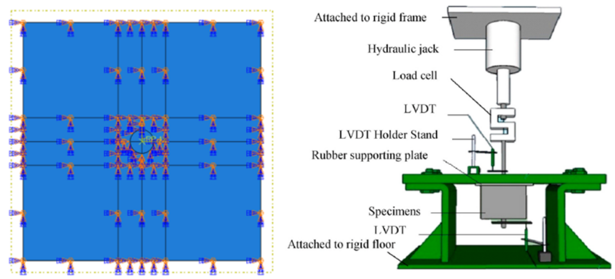

Figure 8: Boundary condition Khaksefidi C4-25-4d and Test setup [23]

Table 4: Mesh size combination for C4-16-6d test sample

Mesh size combination ID	Coarse outer mesh (mm)	Rebar circumference divisions (inner mesh size in mm)
MS1	18	8 div. (6.28)
MS2	15	8 div. (6.28)
MS3	15	12 div. (4.19)
MS4	10	8 div. (6.28)
MS5	10	12 div. (4.19)
MS6	10	16 div. (3.14)

To ensure the FEM results were independent of mesh size, different mesh sizes were evaluated to check the predicted peak loads. A finer mesh density results in greater accuracy during simulations. But this also requires higher computational costs. So, an appropriate mesh size distribution is usually conducted to balance the computational costs and modeling accuracy. Table 4 shows the different mesh size combinations evaluated for C4-16-6d test sample to determine the mesh sensitivity of FEA in this study. Table 5 and Figure 9 shows the load-displacement responses of FEM for each mesh size combination analyzed. Mesh sensitivity analyses carried by comparing peak load capacity and load-displacement responses showed that the adopted mesh sizes produce satisfactorily results.

Table 5: Effect of mesh sizes on C4-16-6d FEM against N_{test} = 85.81 KN

Mesh Size ID	N_{FEM} (KN)	N_{FEM} / N_{test}
MS1	83.613	0.9744
MS2	83.610	0.9744
MS3	84.821	0.9885
MS4	83.610	0.9744
MS5	84.820	0.9885
MS6	85.245	0.9934

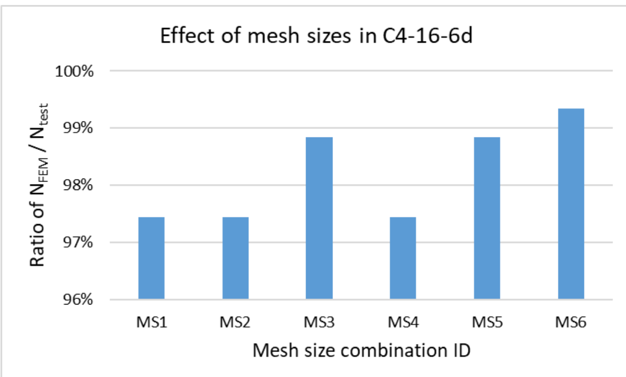

Figure 9: Effect of mesh sizes on peak load capacity in C4-16-6d test sample

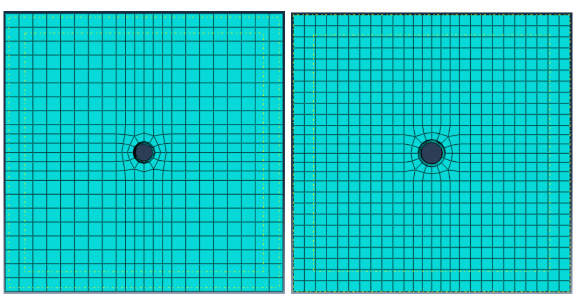

Figure 10: Meshing of C4-16-6d and C4-25-6d with 10 mm outer mesh size

Mesh size was taken as 10 mm outside of 40mm × 40mm section around rebar center. In regions expected to be highly stressed (near circumference of the rebar), the mesh size was taken so as to divide the circumference in 12 segments for 16 mm rebar and 16 segments for 25 mm rebar. This led to a progressive decrease of mesh size to 4.19 mm for 16 mm rebars and 4.91 mm for 25 mm rebars. Figure 10 shows these mesh sizes in C4-16-6d and C4-25-6d models. The results produced from FEM were very close to the reported lab test results. The peak bond strength of rebars agreed quite well between FEM and test results with an average match of 98.625%. The compared peak capacities for four test specimens are shown in Table 6. The load-displacement curves from FEM are compared with test results in Figure 11.

Table 6: Comparison of load capacity in FEM simulation and physical tests by Khaksefidi et al (2021) [23]

Test ID in reference	N_{test} (KN)	N_{FEM} (KN)	N_{FEM} / N_{test} Ratio
C4-16-4d	62.58	61.866	0.989
C4-16-6d	85.81	84.82	0.988
C4-25-4d	132.52	131.736	0.994
C4-25-6d	219.92	214.26	0.974

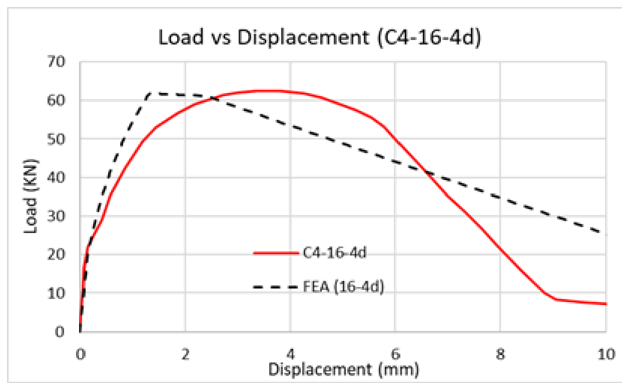

(a) C4-16-4d load-displacement curves

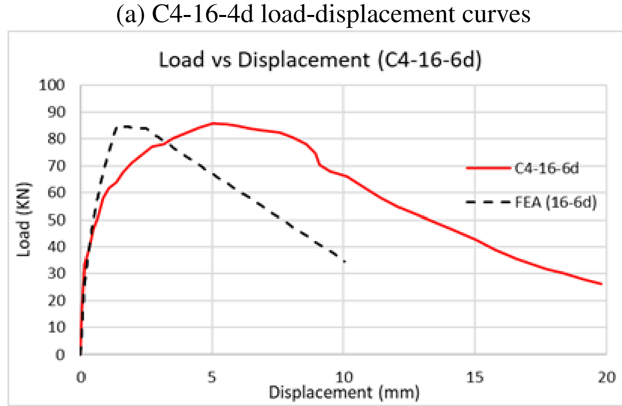

(b) C4-16-6d load-displacement curves

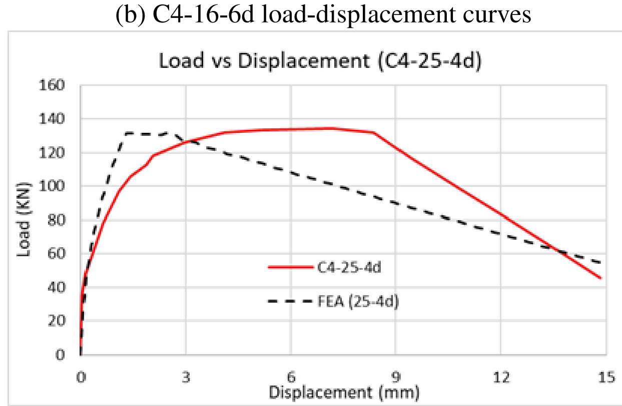

(c) C4-25-4d load-displacement curves

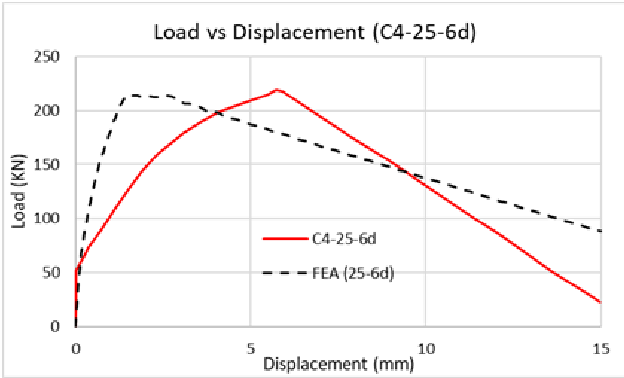

(d) C4-25-6d load-displacement curves

Figure 11: Comparison of load-displacement curves from Khaksefidi et al (2021)

4.2 Reference test for long bond length

For reference tests for long bond length, the experiments conducted by Chicchi, Varma, Seo, Bradt, and McCarty (2020) was taken for FEM [24]. In this study, the researchers considered test results of eight single Rebar Anchor Rods (RARs) and six group RARs for anchorage capacities in tension. The concrete block members were lightly reinforced with supplementary reinforcement to negate flexural and splitting failures of concrete blocks. These supplementary rebars were also modeled as embedded in concrete. The concrete blocks were post-tensioned to the floor near four corners to prevent uplifting. The two tested rebars considered in this study were of 456 MPa yield strength and they had nominal diameters of 19.05 mm.

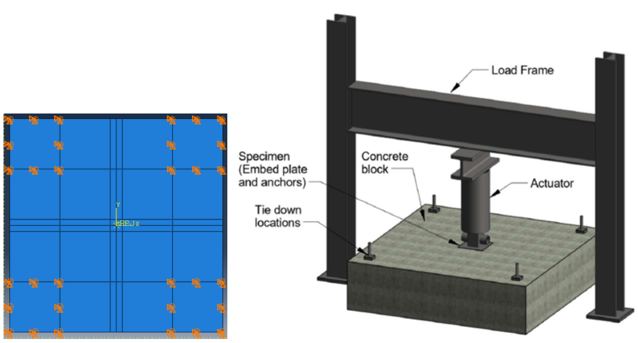

Figure 12: Boundary condition Chicchi S8 and Test setup [24]

The researchers varied the sizes of concrete blocks with tests so that there was no overlap between anchorage breakout cone region (35° angle cone) and post-tensioned bars (45° angle cone). Concrete strength was 30 MPa for S7 and S8 test specimens with the rebar bond lengths as 279mm and 203mm respectively. The reported effective peak bond stresses from the study were used for FEM in this study. Both S7 and S8 specimens were reported to fail by pullout of rebar [24]. Restrictive boundary condition on the four corners of the concrete face near the loading end, as shown in Figure 12 for S8 test specimen model and the test setup.

The restraint offered by post-tensioned tie-down locations holding the concrete block in place was assumed to restrict in translation but not in rotation on the loading end face. For meshing in FEM for long bond lengths, similar approach to the reference tests for short bond lengths was adopted. In regions where higher stresses were expected (near bond region of rebar), finer mesh of approximately 4 - 5 mm was used. In other lesser stressed regions, coarser mesh of 20 mm was used. Mesh sensitivity simulations showed that this mesh size combination produced satisfactory results.

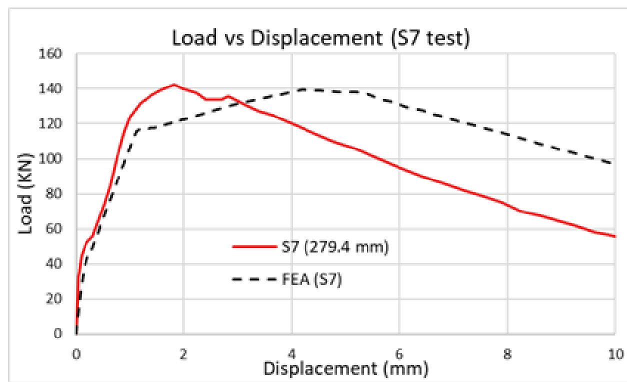

(a) S7 load-displacement curves

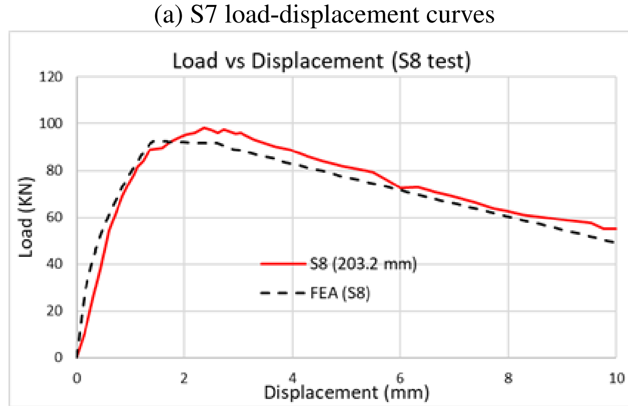

(b) S8 load-displacement curves

Figure 13: Comparison of load-displacement curves from Chicchi et al (2020)

The reported load capacity of S7 was 142.79 KN (i.e., more than the theoretical yield capacity 129.9 KN). This produces a different load-displacement curve for S7 than for S8 as seen in Figure 13. As the peak effective bond is taken based on reported peak capacity, the FEM load capacity is similar to the test capacity for S7 test. For S8 test specimen, the FEM load-displacement curve and peak capacity closely agree with the test result. This was because the failure was by pullout of the rebar. A comparison of load capacity from FEM and tests is made in Table 7. Overall, 95.9% accuracy of predicted FEM capacity against the reported test capacity was seen in average.

Table 7: Comparison of load capacity in FEM simulation and physical tests by Chicchi et al (2020) [24]

Test ID in reference	N_{test} (KN)	N_{FEM} (KN)	N_{FEM} / N_{test} Ratio
S7	142.788	139.39	0.976
S8	98.306	92.55	0.941

4.3 FEM results and limitations

The mesh sensitivity simulations clearly showed that finer meshing around the rebar circumference (bond region) produced a better match of peak load capacity (bond strength) with lab results. The mesh sizes were selected in this study as a balance between computational speed and simulation accuracy. The FEM curve results closely followed the defined bond-slip CZM curve. The values of S_2 and S_3 directly affected the response of bond mechanism in concrete block. The dependence of load-displacement response of FEM on defined bond-slip law observed in this study was also seen in other studies [1, 2, 5]. A better bond-slip law could lead to better load-displacement curve results. Accuracy of FEM prediction against lab results could likely be increased with enhanced numerical techniques to better capture the non-linear behavior of rebar pullout. However, a simple traction-separation law in C3D8R elements is enough to capture the basic response and load capacity of rebars bonded in concrete [1, 2, 17]. The scope of this paper is limited to peak load capacity and overall non-linear load-displacement response of rebars is not studied.

Overall, the results produced by finite element analysis of rebar-concrete bond strength show good match with the reported test results from two different reference test studies. Minor discrepancies are observed in the peak load capacity and the load-displacement responses. Further improvement in FEM results could likely be made with better approximation of the bond-slip relationship between deformed rebar bonded in concrete. Although there is some deviation in the FEM load-displacement curve from the test result curve, the predicted peak load capacity is very close to the reported load capacity with a 98.6% match in Khaksefidi et al (2021) tests and 95.9% match with Chicchi et al (2020) tests.

5. Conclusions

Rebar-concrete bond strength is a structural problem with great consequences for structural safety and stability. The objective of this study was to develop a finite element model capable of predicting bond strength of ordinary steel rebars bonded to concrete based on reference test specimens subjected to pull-out tensile loading. This paper presents the finite element analysis of bond strength of steel reinforcement bars bonded to normal concrete in short bond length and long bond length. Finite element models were created in three-dimensional forms in ABAQUS software, and appropriate material definitions, part geometry definitions, and part interaction properties were defined. A change was made to the standard linear ascending branch in traction separation law by describing a linear branch up to a very small relative displacement of 0.03mm. Then latter branches were described to closely resemble the actual bond-slip law. Then the FEM results are presented in terms of load-displacement curves and peak load capacity. The FEM results are then compared with experimental data reported in the reference studies.

The following conclusions are made as a result of this study:

i) The modified CZM approach used in this study for 3D FEM in ABAQUS can predict the load capacity and bond-slip relation of rebars in concrete quite well. The load-displacement responses and bond strengths predicted by FEM were realistic and matched physical test results.

ii) The results from FEM of rebar bond tests with short as well as long bond lengths show good agreement with the reported experimental test results. FEA showed an average of 98.6% match for short bond length tests conducted by Khaksefidi, Ghalehnovi, and Brito (2021) and 95.9% match for long bond lengths conducted by Chicchi, Varma, Seo, Bradt, and McCarty (2020).

iii) Load-displacement curve obtained from FEM very closely follows the shape of the bond-slip relation defined in the model. When the rebar is stressed above its yield strength, a deviation is observed due to the strain-hardening branch in stress-strain definition of rebar. But in cases where the rebar is stressed below its yield strength, the predicted load-displacement curve is highly dependent on the bond-slip law.

iv) FEM in ABAQUS can be effective in predicting the bond strength of rebars with different bond lengths. Appropriate bond-slip relationship definition and sufficiently fine meshing can satisfactorily replicate physical test results.

v) An improvement in the bond-slip relation definition and finer meshing could lead to even better prediction of bond strength and load-displacement response. Further study is warranted for improvement of FEM accuracy.

References

[1] S. Chapagain, "Performance of steel reinforcement bars as anchor rods," Master's thesis, Pulchowk Campus, Institute of Engineering, Tribhuvan University, December 2023.

[2] C. Boopalan, "Bond behaviour of reinforcing bars embedded in fly ash ggbs based ambient cured geopolymer concrete," Ph.D. dissertation, SRM Institute of Science and Technology, 2022.

[3] S. Seok, G. Haikal, J. A. Ramirez, and L. N. Lowes, "High-resolution finite element modeling for bond in high-strength concrete beam," *Engineering Structures*, vol. 173, pp. 918–932, 2018.

[4] A. S. Genikomsou and M. A. Polak, "Finite element analysis of punching shear of concrete slabs using damaged plasticity model in abaqus," *Engineering structures*, vol. 98, pp. 38–48, 2015.

[5] S. Jeon, M. Ju, J. Park, H. Choi, and K. Park, "Prediction of concrete anchor pull-out failure using cohesive zone modeling," *Construction and Building Materials*, vol. 383, p. 130993, 2023.

[6] B. Wahalathantri, D. Thambiratnam, T. Chan, and S. Fawzia, "A material model for flexural crack simulation in reinforced concrete elements using abaqus," in *Proceedings of the first international conference on engineering, designing and developing the built environment for sustainable wellbeing*. Queensland University of Technology, 2011, pp. 260–264.

[7] A. Rolland, P. Argoul, K. Benzarti, M. Quiertant, S. Chataigner, and A. Khadour, "Analytical and numerical modeling of the bond behavior between frp reinforcing bars and concrete," *Construction and Building Materials*, vol. 231, pp. 117–160, 2020.

[8] D. Darwin, J. Zuo, M. L. Tholen, and E. K. Idun, "Development length criteria for conventional and high relative rib area reinforcing bars," University of Kansas Center for Research, Inc., Tech. Rep., 1995.

[9] G. A. Plizzari, M. A. Deldossi, and S. Massimo, "Transverse reinforcement effects on anchored deformed bars," *Magazine of Concrete Research*, vol. 50, no. 2, pp. 161–177, 1998.

[10] A. C. 408, *ACI PRC-408-03: Bond and development of straight reinforcing bars in tension*. American Concrete Institute, 2003.

[11] H. Lin, Y. Zhao, J. Ozbolt, P. Feng, C. Jiang, and R. Eligehausen, "Analytical model for the bond stress-slip relationship of deformed bars in normal strength concrete," *Construction and Building Materials*, vol. 198, pp. 570–586, 2019.

[12] J. Shafaie, A. Hosseini, and M. Marefat, "3d finite element modelling of bond-slip between rebar and concrete in pull-out test," in *3rd International Conference on Concrete & Development, Iran*, 2009.

[13] X. Gao, N. Li, and X. Ren, "Analytic solution for the bond stress-slip relationship between rebar and concrete," *Construction and Building Materials*, vol. 197, pp. 385–397, 2019.

[14] S. Chapagain and R. Suwal, "Pullout capacity of rebars as anchor rods in nepali construction context," in *14th IOE Graduate Conference Proceedings*, Kathmandu, Nepal, 2023.

[15] M. R. Kabir and M. M. Islam, "Bond stress behavior between concrete and steel rebar: Critical investigation of pull-out test via finite element modeling," *Int J Civ Struct Eng*, vol. 5, no. 1, pp. 80–90, 2014.

[16] K. Senthil, S. Bawa, and C. Aswin, "Influence of concrete strength and diameter of reinforcing bar on pullout tests using finite element analysis," *Journal of Structural Engineering & Applied Mechanics*, vol. 1, no. 3, pp. 105–116, 2018.

[17] ABAQUS, *Abaqus/CAE User's Guide Version 6.14*, United States, 2014.

[18] C. fib, *fib Model Code for Concrete Structures*. Ernst & Sohn, 2013.

[19] X. Yun and L. Gardner, "Stress-strain curves for hot-rolled steels," *Journal of Constructional Steel Research*, vol. 133, pp. 36–46, 2017.

[20] M. Pauletta, N. Rovere, N. Randl, and G. Russo, "Bond-slip behavior between stainless steel rebars and concrete," *Materials*, vol. 13, no. 4, p. 979, 2020.

[21] M. Rezazadeh, V. Carvelli, and A. Veljkovic, "Modelling bond of gfrp rebar and concrete," *Construction and Building Materials*, vol. 153, pp. 102–116, 2017.

[22] X.-B. Luu and S.-K. Kim, "Finite element modeling of interface behavior between normal concrete and ultra-high performance fiber-reinforced concrete," *Buildings*, vol. 13, no. 4, p. 950, 2023.

[23] S. Khaksefidi, M. Ghalehnovi, and J. De Brito, "Bond behaviour of high-strength steel rebars in normal (nsc) and ultra-high performance concrete (uhpc)," *Journal of Building Engineering*, vol. 33, p. 101592, 2021.

[24] R. Chicchi, A. H. Varma, J. Seo, T. Bradt, and E. McCarty, "Experimental testing of tension-loaded deformed anchors in concrete," *ACI Structural Journal*, vol. 117, no. 5, pp. 133–146, 2020.